AIP Applied Physics Letters

Polarization-sensitive microelectromechanical systems based tunable terahertz metamaterials using three dimensional electric split-ring resonator arrays

Fusheng Ma, You Qian, Yu-Sheng Lin, Hongwei Liu, Xinhai Zhang et al.

Citation: Appl. Phys. Lett. **102**, 161912 (2013); doi: 10.1063/1.4803048
View online: http://dx.doi.org/10.1063/1.4803048
View Table of Contents: http://apl.aip.org/resource/1/APPLAB/v102/i16
Published by the American Institute of Physics.

APPLIED PHYSICS LETTERS **102**, 161912 (2013)

Polarization-sensitive microelectromechanical systems based tunable terahertz metamaterials using three dimensional electric split-ring resonator arrays

Fusheng Ma,[1] You Qian,[1] Yu-Sheng Lin,[1] Hongwei Liu,[2] Xinhai Zhang,[2] Zhen Liu,[1] Julius Ming-Lin Tsai,[1,3] and Chengkuo Lee[1,a)]
[1]*Department of Electrical and Computer Engineering, National University of Singapore, Singapore*
[2]*Institute of Materials Research and Engineering, A*STAR, Singapore*
[3]*Institute of Microelectronics, Agency for Science, Technology and Research (A*STAR), Singapore*

(Received 1 February 2013; accepted 12 April 2013; published online 25 April 2013)

We present the design, simulation, fabrication, and characterization of structurally reconfigurable metamaterials showing terahertz frequency tunability with a polarization-sensitivity. The proposed metamaterial structures employ deformable microelectromechanical system based curved cantilevers for tuning the resonance frequency of the electric split-ring resonators. The resonance frequency is observed to be either tunable or non-tunable with the electric field of the incident wave, which is perpendicular or parallel to the split gap of the electric split-ring resonators. This polarization-sensitive characteristic has been demonstrated by both the electromagnetic simulation and the experimental measurement. The observed polarization-sensitive tunability could be used for the development of polarization sensitive and insensitive THz polarimetric devices. © *2013 AIP Publishing LLC* [http://dx.doi.org/10.1063/1.4803048]

Metamaterials, a kind of artificial structures, have attracted intense interests for advanced applications in wide areas.[1–3] These materials exhibit unconventional properties, such as sub-wavelength imaging,[4,5] artificial magnetism,[6–8] field enhancement,[9–12] negative index of refraction,[13–15] and toroidal response.[16] Due to their numerous potential applications, metamaterials have been investigated at radio, microwave, terahertz (THz), infrared, and visible frequencies. As the unique property of THz wave, i.e., transmitting through most natural materials, a plenty of works on metamaterials have been performed in the THz frequency range for potential applications. Moreover, tunable THz metamaterials have also received significant attention because of their potential applications as metadevices.[3] To control the transmission and reflection properties of metamaterials, various methods have been proposed and demonstrated.[17–26] Among these methods, geometrically changing the metamaterial unit cells by using microelectromechanical system (MEMS) based actuators is expected for more drastic change of THz transmission performance.[27–29] Most of the previous works were focused on the planar types, while rare works were reported because of the challenge on fabrication processes for making three dimensional (3D) split-ring resonators (SRRs).[15,30–35] For instance, Zhu *et al*. have demonstrated the planar reconfigurable MEMS based metamaterials using in-plane movable metamaterial unit cells driven by electrostatic comb actuators.[28,29,36] Tao *et al*. have reported a MEMS based metamaterials, in which the SRRs array are supported by two bimorph cantilevers plate.[37,38] Due to the thermal expansion coefficient difference between the two component materials, the two bimorph cantilevers bend upward and lifted up the released metamaterial unit cell plate. The achieved frequency tuning range is less than 0.02 THz with the maximum change of only 45% in transmission intensity.[37] In contrast to the released whole metamaterials layer, Ozbey and Aktas proposed and numerically investigated the MEMS based metamaterials by incorporating a cantilever beam into the electric split-ring resonator structure.[27] They numerically demonstrated the tuning of the resonant frequency of the electric split-ring resonator (eSRR) metamaterial by a magnetically actuated cantilever with a tuning range of 0.2 THz for the low-end of the THz band.[27] As an alternative to coat a magnetic layer on top of the cantilever beams and actuate them with an external magnetic field, the cantilever beams can also be actuated by the electrostatic force. Recently, the polarization dependent transmission properties of metamaterials in terms of anisotropic and bi-anisotropic effects have been investigated for the development of polarimetric devices.[28,39–41]

Thus it is attractive to explore polarization-sensitive tunable mechanisms for THz metamaterials. In this work, we report the polarization sensitive data of the eSRR metamaterial structure using MEMS based single-fixed-end curved cantilever beams to achieve tunable behavior in the THz range. Our findings are critical to the development of polarization sensitive and insensitive THz polarimetric devices.[41] Polarization-sensitive metamaterials, based on their polarization state, provide the possibility for the transmission amplitude or phase control, which shows high promise for polarization isolation and analysis, amplitude and phase modulation, birefringence, and dichroism.

The schematic of the unit cell of the tunable metamaterial eSRR array is shown in Fig. 1(a) with the parameters: the length $w = 80\,\mu$m, the beam width $c = 4\,\mu$m, the gap width $g = 4\,\mu$m, and the width of the capacitor wall $d = 20\,\mu$m. The eSRR structure consists of two rings that share a common "split," and it can be described qualitatively in terms of its

a)Author to whom correspondence should be addressed. Electronic mail: elelc@nus.edu.sg

equivalent circuit with its split and two parallel rings providing capacitance and inductance, respectively.[42] As the two inductive loops are connected in parallel, the resonant frequency of the circuit model is $\omega = \sqrt{2/LC}$. Such a resonator was designed with the capacitive element (the split) coupling strongly to the electric field, while the inductive element (the rings or the loops) does not. The resonance frequency tunability of the eSRR can be achieved by replacing the fixed capacitor with two flexible cantilever beams, i.e., the adjustable deflected shape of cantilever beam will modify the capacitor. Fig. 1(b) shows the unit cell of eSRR with the MEMS-cantilevers bending upwards due to the tensile stress of the bilayer cantilever after releasing. The position of the top end of cantilever beams is denoted by the height h, which will be actuated to change the capacitance of the resonator. Such a kind of 3D metamaterial structure can be realized by the CMOS compatible process and micromachining process. The capacitance of the eSRR structure will depend on the deflected shape of cantilever beams, i.e., the bending angle or height h of the cantilever beams. In order to change the height of the cantilever, force is required to deform the cantilever beam. The flexible free-standing cantilever beam can be actuated by various methods. Here, we use the electrostatic actuation mechanism. The individual eSRR unit cells are electrically connected using conducting metal line in order to electrically connect the entire array of eSRR unit cells forming a two dimensional (2D) eSRR array with the period $P_x = P_y = 120\,\mu$m, schematically depicted in Fig. 1(c). By applying DC bias across the chained and electrically connected eSRR unit cell patterns and silicon (Si) substrate, i.e., ground electrode, the two curved MEMS cantilever beams are bending toward the substrate because of the electrostatic force generated in between. It is worthy to point out that the connecting metal lines have little contribution to the electromagnetic properties of the eSRRs with respect to the normally incident THz electric field.[20] Thus, a straight chain can be made to connect the unit cells to provide a route for the DC bias of electrostatic actuation. The polarization of the incident THz waves is defined as the extraordinary polarization (e-polarization) and ordinary polarization (o-polarization) with reference to the split gaps or

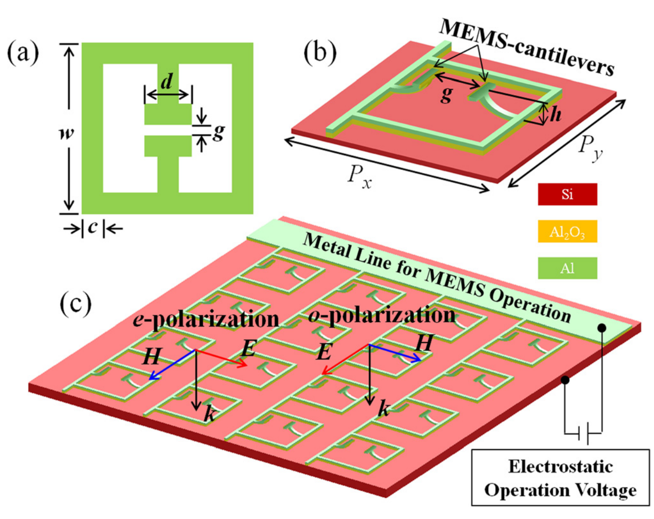

FIG. 1. Schematic diagram with the feature sizes of (a) the unit eSRR cell and (b) the released eSRR cell. (c) The chained eSRR array with a metal line connecting the eSRRs for MEMS operation.

connecting metal lines. For the e-polarization, the electric field is perpendicular to the split gaps, whereas the electric field is parallel to the split gaps in the case of the o-polarization as shown in Fig. 1(c).

The numerical simulations using the finite-different time-domain (FDTD) method were first performed to calculate the transmission spectra and the electromagnetic field distributions corresponding to the resonance modes with the normally incident THz waves of either e- or o-polarization. In the simulation, the periodic structure of the metamaterials was simulated on a single unit-cell by employing periodic boundary conditions in axial directions orthogonal to the incident waves. The structure was excited by using a plane wave incident from the substrate side. To model the influence caused by different positions of the cantilever beams, the height h of the cantilever beams is used to represent the cantilever beam vertical positions under different applied DC voltage. The transmission spectra of the eSRR with the height of the cantilever beams varied from $h = 22$ to $0\,\mu$m are calculated for e- and o-polarized incident THz waves, respectively. The electric and magnetic field strength distribution at the resonance frequencies are also calculated to understand the properties of the resonance modes.

The simulated transmission spectra are shown in Figs. 2(a) and 2(b) for e- and o-polarization incidence, respectively. For the e-polarization incidence as shown in Fig. 2(a), there are two distinct resonances. In this case, the electric field is normal to the "capacitor plates" and thus couples to the capacitive element. The low frequency resonance is the

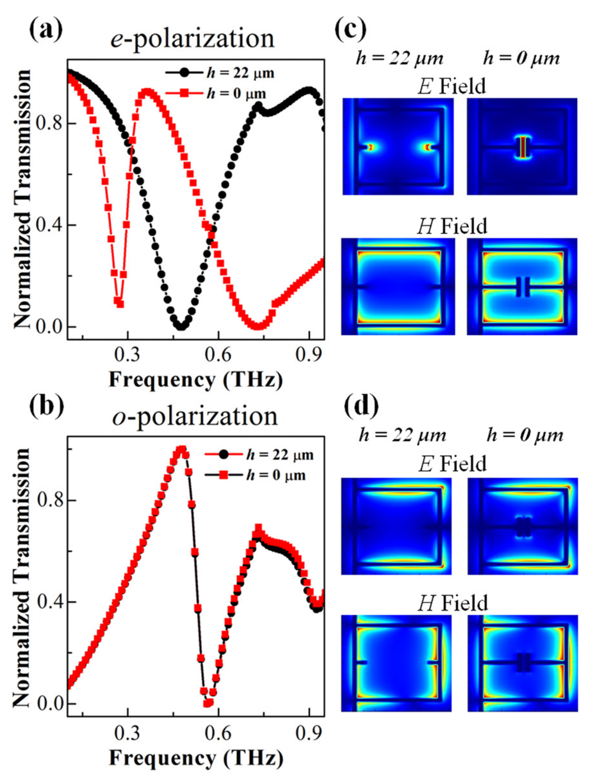

FIG. 2. The simulated transmission spectra of the eSRR array for (a) e-polarization and (b) o-polarization incident light with the cantilever beams height of 22 and $0\,\mu$m, respectively. The electric and magnetic field distribution at (c) LC resonance frequencies for e-polarization and (d) resonance frequencies for o-polarization with the cantilever beams height of 22 and $0\,\mu$m, respectively.

inductive-capacitive (LC) resonance associated with charge accumulation at the gap and oscillating currents in the eSRR loops, while the higher-order resonance is the dipole type electric resonance caused by in-phase dipolar currents along the eSRR sides or components parallel to the incident electric field.[17] This is evidenced by the observation of the calculated electric and magnetic field strength distributed in the eSRR patterns at the fundamental resonance of 0.48 and 0.27 THz when the cantilever beam height $h = 22$ and $0\,\mu$m as shown in Fig. 2(b). The electric field is strongly concentrated at the split gaps, and there is no significant magnetic field distribution along the connecting metal lines between eSRRs at the fundamental resonant frequency, indicating that the eSRR operates in the LC resonant mode. As shown in Fig. 2(a), the displacement of the cantilever beams of the eSRRs is signified by a strong modification of the transmission spectrum for the *e*-polarization. It is found that both the LC resonance and the dipole resonance have a red-shift when the height of the curved cantilever beams changes from 22 to 0 μm. The LC resonance frequency and the dipole resonance frequency are red-shifted from 0.48 to 0.27 THz. This can be understood by the fact that the split gap of the eSRRs decreases to cause an increase of the capacitance, thus reducing the LC resonance from 0.48 to 0.27 THz when the vertical position of the cantilever beam is changed from $h = 22$ to $0\,\mu$m.

In contrast, the transmission spectrum for the *o*-polarization remains practically unchanged when the cantilever beam position changes from $h = 22$ to $0\,\mu$m as shown in Fig. 2(b). In this case, the electric field is parallel to the "capacitor plates" and thus does not couple to the capacitive element. As expected, there is no resonance excited in the LC mode with only one resonance observed from the simulated transmission spectra. This unique resonance results from superimposing the small transmitted intensity of the Drude-like response of the metal lines.[20,43] This kind of resonant response is associated with dipolar currents in the eSRRs as an analog to the higher-lying resonance when the electric field is perpendicular to the connecting metal lines.[20] As shown in Fig. 2(b), the resonance frequency of 0.56 THz is unchanged when the curved cantilever beams bend downward from $h = 22$ to $0\,\mu$m. This is due to the fact that the electric and magnetic field distributions are confined in the eSRR loops rather than along the curved cantilever beams as shown in Fig. 2(d). Therefore, the variation of the vertical position of the curved cantilever beams has trivial effect on the electromagnetic field distribution. Hence, there is no variation of the resonance frequency.

The proposed MEMS based metamaterials, a two-dimensional square-lattice array of eSRR with unit cell of $120 \times 120\,\mu\text{m}^2$, are fabricated by a CMOS compatible process. It is designed to operate in the terahertz range of the spectrum and was characterized from 0.1 to 5 THz. The fabrication process starts with the low-pressure chemical vapor deposition of 100 nm thick silicon oxide, and the silicon oxide layer is then etched by using reactive ion etcher in the square frame region where it becomes the place to form anchors in next step. After that, a 20 nm thick aluminum oxide (Al_2O_3) layer and a 500 nm thick aluminum (Al) layer are deposited using the atomic layer deposition (ALD) and the physical vapor deposition (PVD), respectively. Then, the Al/Al_2O_3 bilayer is patterned with the same mask for metamaterial pattern. Finally, the fabricated eSRR arrays were released using vapor hydrofluoric acid (VHF). Due to the residual tensile stress of Al/Al_2O_3 bilayer, the cantilevers incorporated into the eSRR will bend upwards. The eSRR array with an overall size of approximately $1 \times 1\,\text{cm}^2$ (83×83 unit cells) was fabricated on a silicon wafer. The optical microscope (OM) image for the fabricated eSRR array before release is shown in Fig. 3(a)), and a close-up view of one unit cell is shown in Fig. 3(b). The OM image of the released eSRR array is shown in Fig. 3(c). Fig. 3(d) is the scanning electron microscope (SEM) image of one unit cell of the eSRR array confirming that the cantilever beams are released.

The eSRR metamaterials were characterized by terahertz time domain spectroscopy (THz-TDS, TeraView TPS 3000) in transmission mode. Transmission spectra at two orthogonal polarization states corresponding to the *e*- and *o*-polarization were obtained. In order to experimentally verify the tunability of the metamaterials, the electrostatic operation voltage is applied between the interconnection metal lines merged at the sides of the array and the Si substrate by a DC voltage power supply.

The measured transmission spectra of the fabricated eSRR array with the cantilever beams at various height $h = 22$, 3, and $0\,\mu$m are shown in Figs. 4(a)-4(c) and 4(d)-4(f) as circular dot symbols for *e*- and *o*-polarization incident light, respectively. The observed variation of the resonance frequencies is highlighted by the shaded regions as shown in Fig. 4, where the transmission powers are normalized from the minimum to the maximum. The numerical calculated spectra are also shown in Fig. 4 as solid lines. By comparing the simulation and measurement results in Fig. 4, the THz-TDS measured results are quite consistent with the numerical simulation results. The resonance frequency shifts shown in

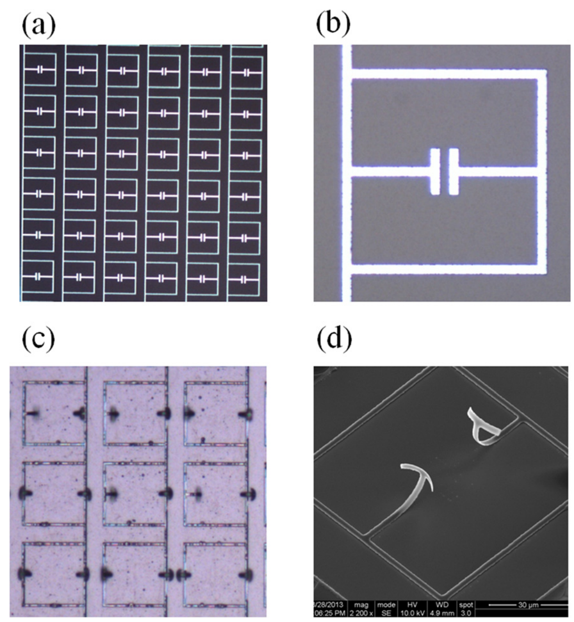

FIG. 3. Optical microscopy image of (a) the unit cell array and (b) the unit cell before release, and (c) the released eSRR array. (d) Scanning electron microscopy image of a unit cell with the cantilever beams released.

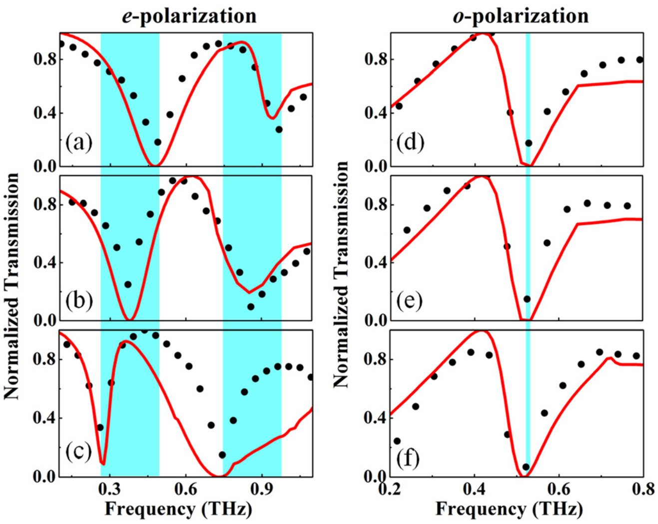

FIG. 4. The measured and simulated transmission spectra of the eSRR array. The first and second columns represent *e*- and *o*-polarization incident light, respectively. The circular symbols and solid lines show the experimentally measured and numerically simulated spectra of transmission, respectively. The shaded regions represent the shift of the resonance frequencies. The first, second, and third rows show the spectra, when the cantilever beam height is (a), (d) 22 μm, (b), (e) 3 μm, and (c), (f) 0 μm.

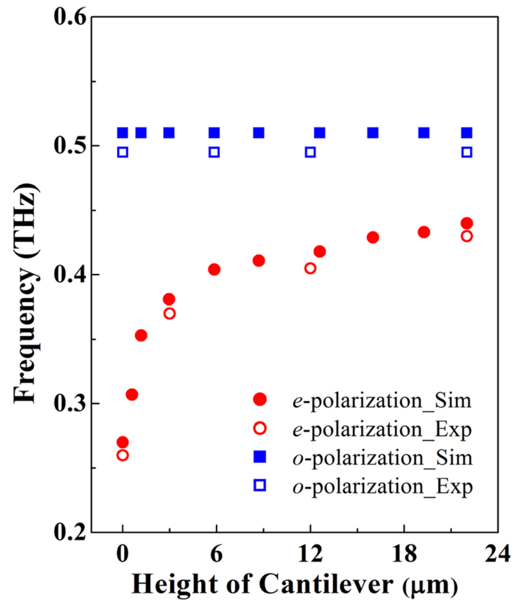

FIG. 5. Dependence of resonant frequency on the cantilever beam height for the proposed devices. The circular and square symbols represent the resonance frequencies for *e*- and *o*-polarization incident light, respectively. The solid and open symbols represent the numerically simulated and experimentally measured values, respectively.

Figs. 4(a)–4(c) are mainly due to the resonance features of the eSRR patterns. As discussed above for *e*-polarization incidence, the electric field strength is mainly confined in the split gap between the two cantilever beams for the LC and dipole resonance modes, whereas the two cantilever beams have trivial effect on the Durde-like resonance for *o*-polarization. Therefore, the changing of the height of the cantilever beams has vital effects on the LC and dipole resonance modes for the *e*-polarization incidence due to the structural change of the split gap between the cantilever beams. Considering the *o*-polarization incidence, however, the position changing of the cantilever beams has trivial effects on the resonance modes when the movable beam is perpendicular to the incident electric field. This explains the different characteristics between *e*- and *o*-polarized incidences of the transmission spectra as a function of cantilever beam positions, which is shown in Fig. 4. As shown in Figs. 4(a)–4(c), for *e*-polarization incidence, the frequency of the LC and dipole resonance decreases from 0.48 to 0.27 THz and from 0.95 to 0.74 THz with a tuning range of 0.21 THz when the height of the cantilever beams varied from $h = 22$ to 0 μm. Such a 0.21 THz tuning range is larger than the reported values using mechanically deforming substrate,[24] temperature control of the permittivity,[44,45] magnetic field tunable superconducting metamaterials,[46] and the MEMS based metamaterials using bimorph cantilevers plate.[37,38] In contrast, the frequency of the Drude-like resonance (0.56 THz) is unchanged for *o*-polarization incident light with the variation of the height of the cantilever beams. Fig. 5 shows the variation of the LC and Durde-like resonance frequency as a function of the cantilever beams actuation height for the *e*- and *o*-polarization, respectively. For the *e*-polarization incidence, it can be seen that the decrease of the LC resonant frequency speeds up with decreasing the cantilever beam height as expected. Since capacitance varies approximately inversely proportional to the spacing, the increase that can be achieved is limited. While for the o-polarization incidence, the resonant frequency does not change with the cantilever beam height variation.

In summary, we proposed a tunable MEMS THz metamaterial by changing the deflected shape of curved cantilever beams simultaneously in an array of eSRR unit cells. Various shapes of curved cantilever beams can be achieved by electric bias such that continuous tuning of the resonance frequency of the eSRR is technically possible. The tunability of the proposed eSRR structures is found to be sensitive to the polarization of the incident THz waves. Reconfiguration of the cantilever beams of the eSRRs is signified by a strong modification of the transmission spectra with a considerable tuning range of 0.21 THz for the *e*-polarization, whereas the transmission spectra for the *o*-polarization remain practically unchanged. This polarization-sensitive characteristic is demonstrated with a good agreement between the numerical simulations and the THz measurement data. Since the resonance frequency of metamaterials structures scales with their feature size, the work performed here at the low-end of the terahertz band can be also applied to the high-end of the terahertz band and over much of the electromagnetic spectrum via appropriate feature size scaling where polarization-sensitive meta-devices may be required.

The authors would like to acknowledge the support by SERC of the Agency for Science, Technology and Research (A*STAR) under Grant No. 1021650084 and the NRF-CRP001-057 Program "Self-powered body sensor network for disease management and prevention-oriented healthcare" under Grant No. R-263-000-A27-281 from National Research Foundation (NRF), Singapore.

[1] N. I. Zheludev, Science **328**, 582 (2010).
[2] N. I. Zheludev, Opt. Photonics News **22**, 30 (2011).
[3] N. I. Zheludev and Y. S. Kivshar, Nat. Mater. **11**, 917 (2012).

[4]J. Pendry, Phys. Rev. Lett. **85**, 3966 (2000).
[5]N. Fang, H. Lee, C. Sun, and X. Zhang, Science **308**, 534 (2005).
[6]J. B. Pendry, A. J. Holden, D. J. Robbins, and W. J. Stewart, IEEE Trans. Microwave Theory Tech. **47**, 2075 (1999).
[7]J. Zhou, T. Koschny, M. Kafesaki, E. N. Economou, J. B. Pendry, and C. M. Soukoulis, Phys. Rev. Lett. **95**, 223902 (2005).
[8]D. Smith, W. Padilla, D. Vier, S. Nemat-Nasser, and S. Schultz, Phys. Rev. Lett. **84**, 4184 (2000).
[9]R. Merlin, Appl. Phys. Lett. **84**, 1290 (2004).
[10]C. E. Talley, J. B. Jackson, C. Oubre, N. K. Grady, C. W. Hollars, S. M. Lane, T. R. Huser, P. Nordlander, and N. J. Halas, Nano Lett. **5**, 1569 (2005).
[11]S. Nie, Science **275**, 1102 (1997).
[12]E. Plum, K. Tanaka, W. T. Chen, V. A. Fedotov, D. P. Tsai, and N. I. Zheludev, J. Opt. **13**, 055102 (2011).
[13]V. M. Shalaev, Nat. Photonics **1**, 41 (2007).
[14]D. R. Smith, J. B. Pendry, and M. C. K. Wiltshire, Science **305**, 788 (2004).
[15]W. T. Chen, C. J. Chen, P. C. Wu, S. Sun, L. Zhou, G. Guo, C. T. Hsiao, K. Yang, N. I. Zheludev, and D. P. Tsai, Opt. Express **19**, 12837 (2011).
[16]T. Kaelberer, V. A. Fedotov, N. Papasimakis, D. P. Tsai, and N. I. Zheludev, Science **330**, 1510 (2010).
[17]W. J. Padilla, A. J. Taylor, and R. D. Averitt, Phys. Rev. Lett. **96**, 107401 (2006).
[18]H. Chen, J. F. O. Hara, A. K. Azad, A. J. Taylor, R. D. Averitt, D. B. Shrekenhamer, and W. J. Padilla, Nat. Photonics **2**, 295 (2008).
[19]J. G. Han, A. Lakhtakia, and C. W. Qiu, Opt. Express **16**, 14390 (2008).
[20]H.-T. Chen, W. J. Padilla, J. M. O. Zide, A. C. Gossard, A. J. Taylor, and R. D. Averitt, Nature (London) **444**, 597 (2006).
[21]H.-T. Chen, S. Palit, T. Tyler, C. M. Bingham, J. M. O. Zide, J. F. O'Hara, D. R. Smith, A. C. Gossard, R. D. Averitt, W. J. Padilla, N. M. Jokerst, and A. J. Taylor, Appl. Phys. Lett. **93**, 091117 (2008).
[22]K. Busch and S. John, Phys. Rev. Lett. **83**, 967 (1999).
[23]E. Ekmekci, A. C. Strikwerda, K. Fan, G. Keiser, X. Zhang, G. Turhan-Sayan, and R. D. Averitt, Phys. Rev. B **83**, 193103 (2011).
[24]J. Li, C. M. Shah, W. Withayachumnankul, B. S. Y. Ung, A. Mitchell, S. Sriram, M. Bhaskaran, S. Chang, and D. Abbott, Appl. Phys. Lett. **102**, 121101 (2013).
[25]M. Kafesaki, N. H. Shen, S. Tzortzakis, and C. M. Soukoulis, J. Opt. **14**, 114008 (2012).
[26]I. V. Munina, V. M. Turgaliev, and I. B. Vendik, Tech. Phys. Lett. **38**, 579 (2012).
[27]Y. S. Lin, Y. Qian, F. S. Ma, Z. Liu, P. Kropelnicki, and C. Lee, Appl. Phys. Lett. **102**, 111908 (2013).
[28]W. M. Zhu, A. Q. Liu, T. Bourouina, D. P. Tsai, J. H. Teng, X. H. Zhang, G. Q. Lo, D. L. Kwong, and N. I. Zheludev, Nat. Commun. **3**, 1274 (2012).
[29]W. M. Zhu, A. Q. Liu, X. M. Zhang, D. P. Tsai, T. Bourouina, J. H. Teng, X. H. Zhang, H. C. Guo, H. Tanoto, T. Mei, G. Q. Lo, and D. L. Kwong, Adv. Mater. **23**, 1792 (2011).
[30]B. D. B. Burckel, J. R. Wendt, G. A. T. Eyck, J. C. Ginn, A. R. Ellis, I. Brener, and M. B. Sinclair, Adv. Mater. **22**, 5053 (2010).
[31]K. Fan, A. C. Strikwerda, H. Tao, X. Zhang, and R. D. Averitt, Opt. Express **19**, 12619 (2011).
[32]R. A. Shelby, D. R. Smith, and S. Schultz, Science **292**, 77 (2001).
[33]C. M. Soukoulis and M. Wegener, Science **330**, 1633 (2010).
[34]C. C. Chen, C. T. Hsiao, S. Sun, K.-Y. Yang, P. C. Wu, W. T. Chen, Y. H. Tang, Y.-F. Chau, E. Plum, G.-Y. Guo, N. I. Zheludev, and D. P. Tsai, Opt. Express **20**, 9415 (2012).
[35]Z. C. Chen, R. Mohsen, Y. D. Gong, C. T. Chong, and M. H. Hong, Adv. Mater. **24**, OP143 (2012).
[36]A. Q. Liu, W. M. Zhu, D. P. Tsai, and N. I. Zheludev, J. Opt. **14**, 114009 (2012).
[37]H. Tao, A. Strikwerda, K. Fan, W. Padilla, X. Zhang, and R. Averitt, Phys. Rev. Lett. **103**, 147401 (2009).
[38]H. Tao, A. C. Strikwerda, K. Fan, W. J. Padilla, X. Zhang, and R. D. Averitt, J. Infrared Milli. Terahz. Waves **32**, 580 (2011)
[39]R. Marqués, F. Medina, and R. Rafii-El-Idrissi, Phys. Rev. B **65**, 144440 (2002).
[40]X. Xu, B. Quan, C. Gu, and L. Wang, J. Opt. Soc. Am. B **23**, 1174 (2006).
[41]X. G. Peralta, E. I. Smirnova, A. K. Azad, H.-T. Chen, A. J. Taylor, I. Brener, and J. F. O'Hara, Opt. Express **17**, 773 (2009).
[42]D. Schurig, J. J. Mock, and D. R. Smith, Appl. Phys. Lett. **88**, 041109 (2006).
[43]J. Pendry, A. Holden, W. Stewart, and I. Youngs, Phys. Rev. Lett. **76**, 4773 (1996).
[44]H. Němec, P. Kužel, F. Kadlec, C. Kadlec, R. Yahiaoui, and P. Mounaix, Phys. Rev. B **79**, 241108 (2009).
[45]R. Singh, A. K. Azad, Q. X. Jia, A. J. Taylor, and H.-T. Chen, Opt. Lett. **36**, 1230 (2011).
[46]C. H. Zhang, J. B. Wu, B. B. Jin, Z. M. Ji, L. Kang, W. W. Xu, J. Chen, M. Tonouchi, and P. H. Wu, Opt. Express **20**, 42 (2012).